

Structure of photosynthetic LH1-RC super-complex at 1.9 Å resolution

Long-Jiang Yu¹, Michihiro Suga¹, Zheng-Yu Wang-Otomo², Jian-Ren Shen^{1,*}

¹Research Institute for Interdisciplinary Science, and Graduate School of Natural Science and Technology, Okayama University, Japan

²Faculty of Science, Ibaraki University, Japan

*Corresponding author

ABSTRACT

Light-harvesting-1 (LH1) and reaction center (RC) core complex is an integral membrane-protein super-complex of purple photosynthetic bacteria that performs the primary reactions of photosynthesis. The structure of LH1-RC has been reported at relatively low resolutions, providing much information on the arrangement of protein subunits and cofactors. Here we report the crystal structure of a Ca-bound LH1-RC super-complex from *Thermochromatium tepidum* at a resolution of 1.9 Å. This atomic resolution structure revealed a number of novel features regarding the organization of protein subunits and cofactors, allowing us to identify some RC loop regions in their intact states and their interactions with the LH1 subunits, the exchange route for the bound Q_B with the free quinones as well as for their transport between inside and outside of the LH1 ring structure, and the detailed Ca^{2+} -binding environment. This structure provides a solid basis for detailed examination of the light reactions of bacterial photosynthesis.

Photosynthesis converts light energy from the sun into biologically useful chemical energy, thereby sustaining virtually all life forms on the earth. Purple photosynthetic bacteria possess a simple and robust photosynthetic apparatus, which has been extensively studied regarding the initial photochemical reactions¹. In most purple photosynthetic bacteria, there are typically two kinds of light-harvesting (LH) complexes LH1 and LH2, where light energy is first absorbed by the peripheral LH2, then transferred via LH1 rapidly and efficiently to the reaction center (RC) to drive the primary redox reactions. LH1 exists in all purple bacteria and surrounds the RC to form an integral membrane protein-pigment super-complex (LH1-RC) consisting of 32-36 subunits with a total molecular weight of ~400 kDa.

The structures of the Ca²⁺-bound and the Sr/Ba substituted LH1-RC super-complexes have been determined at 3.0 Å and 3.3 Å resolutions from a thermophilic purple sulfur photosynthetic bacterium *Thermochromatium (Tch.) tepidum*^{2,3}, respectively, which showed that the RC is surrounded by 16 heterodimers of the LH1 α , β -subunits containing 32 bacteriochlorophyll (BChl) *a* and 16 spirilloxanthin (Spx) molecules, forming a completely closed elliptical ring. This is different from the structure of LH1-RC dimers from *Rhodobacter (Rb.) sphaeroides* and monomers from *Rhodospseudomonas (Rps.) palustris* determined by X-ray diffraction at 8.0 Å⁴ and 4.8 Å⁵ resolutions, in that both of them show an incomplete ring structure with the dimer having a PufX subunit and the monomer having a protein W, respectively, in their ring openings. Furthermore, 16 Ca²⁺ binding sites were observed in the C-terminal loop region of the thermophilic LH1 complex, which was considered the reason for the unusual redshift and enhanced thermal stability of the thermophilic LH1^{6,7}.

The resolution of the structure of LH1-RC reported so far, however, was not enough to reveal the detailed organization of many cofactors involved in the energy and electron transfer reactions within this super-complex. Here we report the structure of LH1-RC from *Tch. tepidum* at 1.9 Å resolution, which revealed detailed arrangement and organization of a large number of cofactors including BChls, carotenoids, menaquinone (MQ8) and ubiquinones (UQ8), lipids, Ca²⁺ and water molecules. On the basis of the high-resolution structure, energy transfer from LH1 to RC, quinone and proton channels, possible roles of Ca²⁺ are examined. These results greatly advance our understanding on the bacterial photosynthetic light reactions.

Overall structure

The quality of the LH1-RC crystals was improved significantly by optimization of the detergent and other conditions of crystallization, enabling the structure to be resolved at

1.9 Å resolution (Extended Data Fig. 1 and 2, Extended Data Table 1). The space group of the crystal obtained was *C2*, which is the same as that reported in the previous study² (Extended Data Fig. 1c, d). However, the unit cell dimensions were much shorter than those of the previous one (Extended Data Table 1), leading to a more compact packing and a much less solvent content of 55% compared to 65% for the previous crystals². This may be the major reason for the significant improvement in the crystal resolution.

The overall structure of the LH1-RC core complex is largely similar to that of the previous one determined at 3.0 Å resolution² (Fig. 1). However, the root mean square deviation (rmsd) between C α atoms of the two structures is 1.68 Å; this relatively large rmsd is mainly caused by deviations in some regions of the RC subunits and the N-, C-termini of the LH1 subunits (see below). We identified a number of lipid and detergent molecules in the gap region between RC and LH1 (Fig. 1c), resulting in a rather crowded 'gap region' in comparison with the previous rather empty gap space (Extended Data Fig. 3). The whole structure contained 4 protein subunits, 4 BChls *a*, 2 bacteriopheophytins (BPheos), 1 Mg²⁺ ion, 1 Fe³⁺ ion, 1 Spx molecule, 1 MQ8 and 5 UQ8s in RC, and 16 pairs of LH1 α , β -subunits, 32 BChls *a* and 16 Spx molecules, 16 Ca²⁺ ions in LH1 (Fig. 1, Extended Data Table 2). In addition, nearly 1,000 water molecules were found in the super-complex, which are mostly distributed in both the cytoplasmic and periplasmic, hydrophilic surfaces (Fig. 1b). The overall shape of the LH1-RC super-complex is an ellipse as has been reported, and the LH1-BChls have almost equa-distances to the RC BChls (Fig. 1d). This may ensure an efficient energy transfer from LH1 to RC.

The rmsds between the C α atoms of the new RC structure and the RC-only structure at 2.2 Å resolution⁸, or the RC structure at 3.0 Å resolution², were 3.19 Å and 1.98 Å, respectively, due to the apparent differences in some regions of the RC structures (Extended Data Figs. 3b, 4). In addition, the C-terminal loop regions of all α -apoproteins of LH1, which has poor electron densities in the previous 3.0 Å structure², show relatively large deviations (Extended Data Fig. 4c, 4d). Since these terminal regions are exposed to the surface of the membrane and partly flexible as manifested in their high B-factors (Extended Data Table 3), we adjusted the length of the α/β -apoproteins with confidence based on the electron density map. Furthermore, the position and coordination patterns for the calcium ions were identified unambiguously. In the following, we describe features found in the present high-resolution structure that are unique and important for the functionality of this super-complex.

Unique features in the structure of RC

Comparison of our structure with those of the isolated RC reported previously revealed

three major differences; they include the N-terminal region in the Cyt subunit and its loop region (residues 172–196), and a loop region in the H subunit (residues 44–58) (Fig. 2a, 2c, 2d). Cyt C is located at the periplasmic side, and has been reported to be a lipoprotein in *Blastochloris (Bl.) viridis* with its N-terminal cysteine linked to a diglyceride via a thioether bond⁹⁻¹¹. In the previous structure², this region was assigned incorrectly because of the lower resolution or possible X-ray radiation damage that may break the thioether bond¹¹. In the present structure, the electron density map showed three partial acyl chains attached to the Cyt C-Cys23, among which, one is a single chain and the other one is clearly branched (Fig.2b). This suggests that Cyt is triacylated at the N-terminal cysteine with N-acyl and S-diacylglycerol similar to an outer membrane protein¹², and these fatty acids anchor the Cyt subunit in the membrane. All aliphatic tails beyond the seventh carbon from the carbonyl carbon are disordered, presumably due to their flexibility, and could interact with the UQ8 found in the position waiting for the exchange of Q_B (see below). In addition, the loop region (172–196) of Cyt showed a large deviation from that of the isolated RCs^{8,9}, which appears to interact with the neighboring LH1 only in this conformation (Fig. 2c). A Mg²⁺ ion was found in its vicinity (Fig. 2c, 2e), which may reduce the flexibility of this long loop.

The loop region (44–58) of the H subunit was traced unambiguously in the present structure (Fig. 2d), which interacts with the neighboring LH1 β -polypeptide at the cytoplasmic side. This is largely different from the isolated RCs and the previous LH1-RC. For example, these residues are located in the crystal lattice contact region in the recently reported RC structure from *Bl. viridis* at 1.92 Å⁹, which differs from the previous structures^{11,13}. Thus, the interactions with the LH1 polypeptide appear to be required to keep this region in the correct configuration.

Quinones and lipids

One MQ8 and five UQ8s were found in the LH1-RC super-complex (Fig. 3a), which is consistent with the results of biochemical analysis with the same sample¹⁴. Among these quinones, MQ8 and one of the UQ8 function as Q_A and Q_B with similar binding sites as those reported previously². The additional UQ8s were found to be distributed over RC and in the gap region between RC and LH1. In particular, one of the UQ8 was located in a position close to the isoprenoid tail of Q_B near the periplasmic surface (Fig. 3a), with its head oriented in the same direction as that of Q_B, suggesting that this quinone is in a position waiting for the exchange of Q_B following its double reduction and protonation. This is supported by the fact that, while the head of Q_B is surrounded by a number of residues and hydrogen-bonded to L-His199, L-Ser232, L-Ile233 and L-Gly234, the head

of the second UQ8 was not hydrogen-bonded to any residues, and its isoprenoid tail was not visible, presumably due to its high flexibility (Fig. 3a). The cavity harboring the head of this UQ8 was formed by L-Met183, L-Leu184, L-Ser187, L-Trp272, M-Ile179, as well as accessory BChl bound to the M subunit.

Three UQ8s are located in the gap region between LH1 and RC, among which, two are close to the LH1 ring and the isoprenoid tail of one of these two UQ8s was found to be inserted into a space between the LH1 α - and β -subunits (Fig. 3b, 3c), suggesting that it is on the way to be transported between the inside and outside of the ring structure through the possible exchange channel in LH1 subunits. This channel is close to the cytoplasmic side of the membrane at the same level as the Q_B head, and has been suggested in the previous study^{2,15}, but our present result provides direct evidence for the transport of quinones through such channels. This channel is hydrophobic and surrounded by Val20, Ser23, Ile24 and Phe27 from an α -subunit of LH1 in one side, and Leu21, Val22, Val25 and Ile29 from another α -subunit in the opposite side (Fig. 3c). In addition, the Spx and phytol tail of BChl bound to the LH1 α -subunit are close to the exit of the channel, which may contribute to form the hydrophobic channel exit.

Extensive hydrogen-bond networks in the H subunit connecting Q_B to the cytoplasmic surface (Extended Data Fig. 5) were found, owing to the large number of water molecules identified. One of the major hydrogen-bond networks is approximately normal to the membrane surface, and may serve as a possible proton transfer channel connecting Q_B to the aqueous phase¹⁶. We also found a water cluster parallel to the membrane plane similar to that found in *Rb. sphaeroides* RC¹⁶⁻¹⁸. These hydrogen-bond networks may support the idea that there is multi-entry proton uptake networks for the protonation of Q_B¹⁹.

Among the 21 lipids identified, nine are tentatively assigned to cardiolipins (CDLs), ten to phosphatidylglycerols (PGs) and two to phosphatidylethanolamines (PEFs) (Supplementary Table 2, Fig. 3d). This number is much larger than that found in the RC-only structure where only 1-2 lipids were found, presumably due to the loss or disorder of the lipid molecules upon solubilization of the RC-only complex, or replacement by the detergents employed. The distribution of the lipids is asymmetric: all of the CDLs were found at the cytoplasmic side with their head groups localized at the surface of the membrane, whereas PEF and PG were located at both cytoplasmic and periplasmic sides. All of the three lipids previously reported at 3.0 Å resolution were confirmed with some modifications in that, the PEF and one of the two PGs were re-assigned as CDL and PEF, respectively.

Interactions of LH1-RC and among LH1

The interactions between LH1 and RC are found at both periplasmic and cytoplasmic sides either directly (Fig. 4a, 4b) or indirectly (through lipids etc, Extended Data Table 4). As mentioned above, the newly built loop region (172-196) of Cyt forms two hydrogen bonds between Cyt C-Ser176, C-Gly177 and the neighboring α -Asp48, α -Ser41, which may stabilize this region of the Cyt C-subunit, indicating that this conformation represents its intact state. In addition, M-Leu109, C-Arg47, L-Arg85, and H-His7 interact with the neighboring LH1 α -Ser41 or α -Asp48 at the periplasmic side (Extended Data Fig. 6a, 6b, 6c). Importantly, α -Ser41 and α -Asp48 are two main residues for the interaction between LH1 and RC subunits or lipids at the periplasmic side (Extended Data Table 4). At the cytoplasmic side, two arginine residues Arg18/Arg19 located at the beginning of the α -subunit helices play the major role in interacting with the RC subunits or lipids, and some other residues (H414, Asp16 and Ser23) also provided some interactions with RC and lipids (Fig. 4b, Extended Data Fig. 6d-f, Extended Data Table 4). These two arginines form a positively charged layer together with some other arginines/lysines from the RC and α -Lys10/ β -Lys15 at the membrane surface, which may interact with the phosphate group of the lipids and thereby strength the association of LH1 with RC.

Extensive interactions between the LH1 α/β -heterodimers are found around the Ca-binding site in the C-terminal domain at the periplasmic side, especially in the region of the residues α -42~49 (Fig. 4c). This region forms a characteristic short turn structure at the surface of the membrane, which occurs in *Tch. tepidum* only, since a residue at the position 43 is deleted in this organism in comparison with other photosynthetic bacteria²⁰. This characteristic structure enables α -Asp43 to form hydrogen bonds with α -Asp48, α -Ser54, α -Tyr55 and α -Gln56 from the neighboring α -polypeptide. In addition, α -Asn45 is also a key residue since it is conserved in almost all purple bacteria, and forms extensive interactions with its neighboring subunits. β -Arg43 is also highly conserved and involved in additional interactions with its neighboring subunits (Extended Data Table 4). Another strong hydrogen-bond responsible for the α/β -interactions was found between β -Pro44 and α -Tyr55. On the other hand, only one strong hydrogen bond was found between β -Leu46 and (n-1) β -Tyr42 at the membrane surface for the β/β interactions.

In contrast to the extensive interactions in the C-terminal region at the periplasmic side, those in the N-terminal region at the cytoplasmic side are less, where β -Thr7 is hydrogen-bonded with α -Leu13 and α -Trp12 respectively, and β -Asp11 interacts with α -Tyr9 and α -Lys10 respectively (Fig. 4c). Taken together, the interactions in both the N-terminal and C-terminal regions ensure a tight connection of the LH1 α/β -apoproteins as well as a joint coordination to BChls *a*, carotenoids and Ca^{2+} ions (Fig. 5a, 5b, see below), which results in a robust structural unit as a closed concentric elliptical ring.

Ca²⁺ binding sites

One of the remarkable features of the thermophilic LH1-RC is its binding of 16 Ca²⁺ ions in the LH1 subunits, and we identified all of the ligands for Ca²⁺ unambiguously, which are the side chain of α -Asp49, the carbonyl oxygens of α -Trp46, α -Ile51, (n+1) β -Trp45, and two water molecules, giving rise to a six-coordinated structure (Fig. 5c, 5d). Three out of the four coordinating residues are hydrophobic; this may be due to the fact that this binding site is located just at the periplasmic surface of the membrane, and may thus contribute to its weak binding, making it easily exchangeable with other divalent cations^{21,22}.

The Ca²⁺-binding site is located in the C-terminal region of both α/β -subunits, which contributed to the tight connection of the two LH1 subunits (Fig. 5). This is in accordance with the result of FTIR measurement which showed that Ca²⁺-binding reduces the conformational flexibility of LH1-RC²³. The structural stability induced by the binding of Ca²⁺ may therefore contribute to the thermophilic stability of LH1 as well as the red shift of the absorption peak, two unique features of the thermophilic bacterium. These results are in agreement with those of recent spectral measurements²⁴⁻²⁶.

The unique binding of Ca²⁺ may be related to the deletion of the residue α -43 in *Tch. tepidum*²⁰, since insertion of an Ala into this site has been shown to disrupt the Ca²⁺-binding of the thermophilic LH1, leading to a blue shift in its absorption²⁷. This is consistent with the Ca²⁺-binding environment revealed in the present study and its functional importance.

Apparent differences were also found in BChls of LH1 in comparison with the previous 3.0 Å structure. The imidazole ring of β -His36, a direct ligand to β -BChl, is rotated by about 45 degrees in most cases; and the porphyrin plane of the β -BChl is rotated by about 10 degrees along its Qy axis. These changes resulted in a more parallel orientation of the neighboring BChls, giving rise to a stronger coupling between the adjacent BChls.

Acknowledgements

We thank M. T. Madigan for providing the *Tch. tepidum* strain MC, F. Ma, Y. Xin, Y. Umena, X. Chen, X. Qin, W. Wang and T. Kawakami for kind discussions and helps during the experiments, data analysis and manuscript preparation. This work was supported by JSPS KAKENHI No. JP24000018 and JP17H0643419 (to J.-R.S.), JP16H04174 (to Z.-Y.W.-O.), JP16H06296 and JP16H06162 (to M.S.), a program for promoting the enhancement of research universities at Okayama University from MEXT, Japan, and performed using the beamlines BL41XU (proposal numbers 2014B1277, 2015A1079, 2015B2079, 2016A2553, 2017A2590 to L.-J.Y.), BL44XU (2015B6522, 2016A6621, 2016B6621, 2017A6724, 2017B6724 to M.S.) at SPring-8, and BL-1A at Photon Factory (PF), Japan (2016R-27 to L.-J.Y.). We are grateful to staff members of SPring-8 and PF for their assistance in the data collection.

Author Contributions

J.-R. S. and L.-J. Y. conceived the project; L.-J. Y. prepared the samples with the help of Z.-Y. W.-O., grew the crystals, L.-J.Y. and M.S. collected the diffraction data and analyzed the structure; L.-J.Y. and J.-R. S. wrote the manuscript, and all authors contributed to the discussion and improvement of the manuscript.

Author Information

The structure factors and coordinates have been deposited in Protein Data Bank with an accession code 5Y5S. The authors declare no competing financial interests. Readers are welcome to comment on the online version of the paper. Correspondence and requests for materials should be addressed to J.-R. S. (shen@cc.okayama-u.ac.jp).

References

1. Cogdell, R. J. & Roszak, A. W. Structural biology: The purple heart of photosynthesis. *Nature* **508**, 196-197 (2014).
2. Niwa, S. *et al.* Structure of the LH1-RC complex from *Thermochromatium tepidum* at 3.0 Å. *Nature* **508**, 228-232 (2014).
3. Yu, L. J., Kawakami, T., Kimura, Y. & Wang-Otomo, Z. Y. Structural basis for the unusual Qy red-shift and enhanced thermostability of the LH1 complex from *Thermochromatium tepidum*. *Biochemistry* **55**, 6495-6504 (2016).
4. Qian, P. *et al.* Three-dimensional structure of the *Rhodobacter sphaeroides* RC-LH1-PufX complex: dimerization and quinone channels promoted by PufX. *Biochemistry* **52**, 7575-7585 (2013).
5. Roszak, A. W. *et al.* Crystal structure of the RC-LH1 core complex from *Rhodospseudomonas palustris*. *Science* **302**, 1969-1972 (2003).
6. Kimura, Y. *et al.* Calcium ions are involved in the unusual red shift of the light-harvesting 1 Qy transition of the core complex in thermophilic purple sulfur bacterium *Thermochromatium tepidum*. *J. Biol. Chem.* **283**, 13867-13873 (2008).
7. Kimura, Y., Yu, L. J., Hirano, Y., Suzuki, H. & Wang, Z. Y. Calcium ions are required for the enhanced thermal stability of the light-harvesting-reaction center core complex from thermophilic purple sulfur bacterium *Thermochromatium tepidum*. *J. Biol. Chem.* **284**, 93-99 (2009).
8. Nogi, T., Fathir, I., Kobayashi, M., Nozawa, T. & Miki, K. Crystal structures of photosynthetic reaction center and high-potential iron-sulfur protein from *Thermochromatium tepidum*: thermostability and electron transfer. *Proc. Natl. Acad. Sci. USA* **97**, 13561-13566 (2000).
9. Roszak, A. W. *et al.* New insights into the structure of the reaction centre from *Blastochloris viridis*: evolution in the laboratory. *Bioch. J.* **442**, 27-37 (2012).
10. Weyer, K. A., Schafer, W., Lottspeich, F. & Michel, H. The cytochrome subunit of the photosynthetic reaction center from *Rhodospseudomonas viridis* is a lipoprotein. *Biochemistry* **26**, 2909-2914 (1987).
11. Wohri, A. B. *et al.* Lipidic sponge phase crystal structure of a photosynthetic reaction center reveals lipids on the protein surface. *Biochemistry* **48**, 9831-9838 (2009).
12. Kulathila, R., Kulathila, R., Indic, M. & van den Berg, B. Crystal structure of *Escherichia coli* CusC, the outer membrane component of a heavy metal efflux pump. *Plos One* **6**, e15610 (2011).
13. Li, L. *et al.* Nanoliter microfluidic hybrid method for simultaneous screening and optimization validated with crystallization of membrane proteins. *Proc. Natl. Acad.*

- Sci. USA* **103**, 19243-19248 (2006).
14. Kimura, Y. *et al.* Characterization of the quinones in purple sulfur bacterium *Thermochromatium tepidum*. *FEBS letters* **589**, 1761-1765 (2015).
 15. Wang-Otomo, Z.-Y. in *Solar to Chemical Energy Conversion*. (eds. Sugiyama, M. *et al.*), pp. 379-390 (Springer, 2016).
 16. Stowell, M. H. B. *et al.* Light-induced structural changes in photosynthetic reaction center: Implications for mechanism of electron-proton transfer. *Science* **276**, 812-816 (1997).
 17. Fritsch, G., Kampmann, L., Kapaun, G. & Michel, H. Water clusters in the reaction centre of *Rhodobacter sphaeroides*. *Photosynth Res* **55**, 127-132 (1998).
 18. Abresch, E. C. *et al.* Identification of proton transfer pathways in the X-ray crystal structure of the bacterial reaction center from *Rhodobacter sphaeroides*. *Photosynth. Res.* **55**, 119-125 (1998).
 19. Krammer, E. M., Till, M. S., Sebban, P. & Ullmann, G. M. Proton-transfer pathways in photosynthetic reaction centers analyzed by profile hidden markov models and network calculations. *J. Mol. Biol.* **388**, 631-643 (2009).
 20. Rucker, O., Kohler, A., Behammer, B., Sichau, K. & Overmann, J. Puf operon sequences and inferred structures of light-harvesting complexes of three closely related Chromatiaceae exhibiting different absorption characteristics. *Arch. Microbiol.* **194**, 123-134 (2012).
 21. Kimura, Y., Inada, Y., Yu, L. J., Wang, Z. Y. & Ohno, T. A spectroscopic variant of the light-harvesting 1 core complex from the thermophilic purple sulfur bacterium *Thermochromatium tepidum*. *Biochemistry* **50**, 3638-3648 (2011).
 22. Kimura, Y. *et al.* Metal cations modulate the bacteriochlorophyll-protein interaction in the light-harvesting 1 core complex from *Thermochromatium tepidum*. *Biochim. Biophys. Acta* **1817**, 1022-1029 (2012).
 23. Jakob-Grun, S., Radeck, J. & Braun, P. Ca²⁺-binding reduces conformational flexibility of RC-LH1 core complex from thermophile *Thermochromatium tepidum*. *Photosynth. Res.* **111**, 139-147 (2012).
 24. Ma, F., Yu, L. J., Wang-Otomo, Z. Y. & van Grondelle, R. The origin of the unusual Qy red shift in LH1-RC complexes from purple bacteria *Thermochromatium tepidum* as revealed by Stark absorption spectroscopy. *Biochimica et biophysica acta* **1847**, 1479-1486 (2015).
 25. Ma, F., Yu, L. J., Wang-Otomo, Z. Y. & van Grondelle, R. Temperature dependent LH1-->RC energy transfer in purple bacteria *Tch. tepidum* with shiftable LH1-Q band: A natural system to investigate thermally activated energy transfer in photosynthesis.

Biochim Biophys. Acta **1857**, 408-414 (2015).

26. Ma, F. *et al.* Metal cations induced alpha, beta-BChl *a* heterogeneity in LH1 as revealed by temperature-dependent fluorescence splitting. *Chemphyschem.* **18**, 2295-2301. (2017).
27. Nagashima, K. V. P. *et al.* Probing structure-function relationships in early events in photosynthesis using a chimeric photocomplex. *Proc. Natl. Acad. Sci. USA* **114**, 10906-10911 (2017).

Figure legends

Figure 1 | Architecture of the LH1-RC complex from *Tch. tepidum* at a resolution of 1.9 Å. **a**, View from the direction parallel to the membrane plane. **b**, Arrangement of the cofactors and water molecules with the same view as in panel **a**. **c**, Arrangement of the cofactors with a view perpendicular to the membrane. Protein subunits are depicted in light grey. **d**, Distances between the closest pairs of Bchls between LH1 and RC. Color codes for cofactors: green, Bchls; yellow, Spx; orange balls, Ca²⁺ ions; raspberry dots, water molecules. Color codes for proteins in panel **a**: blue, LH1 α -subunit; light cyan, LH1 β -subunit; purple, RC C-subunit.

Figure 2 | Differences between the structures of isolated and intact RC core. **a**, Superposition of the isolated RC structures from *Tch. tepidum* (1EYS; purple), *Rb. sphaeroides* (2J8C; orange), *Bl. viridis* (3T6E; yellow) and the present one (marine). Regions with similar structures are colored in grey, whereas the three regions with large differences are boxed and colored differently. The boxed areas numbered 1, 2, 3 are enlarged in **b**, **c** and **d**, respectively. **b**, Tri-acylation of the Cyt N-terminal cysteine. **c**, The loop region of Cyt (residues 172-196) including the Mg²⁺-binding site, which is circled in **c** and enlarged in **e**. **d**, The N-terminal region and residues 44-58 of the H subunit. **e**, The Mg²⁺-binding site in the Cyt subunit.

Figure 3 | Distribution of quinones and lipids in the LH1-RC. **a**, Overall distribution of the six quinones revealed in the present structure. Color codes: green, UQs, cyan, MQ, red, UQ with its tail inserted in the channel between the LH1 α/β -subunits. Orange and blue, two α - and two β -subunits of LH1 that form the channel for the transport of the UQ. **b**, **c**, Quinone exchange channel between the LH1- α/β subunits. **d**, Distribution of lipids with a side view of the LH1-RC super-complex. The lipid molecules are shown in space-filling mode (oxygen, red; nitrogen, blue; carbons of PEF, CDL and PG are colored in green, yellow and magenta, respectively, and protein subunits in grey).

Figure 4 | Interactions between LH1 and RC, and among LH1. For clarity, only protein-protein interactions are depicted. **a**, Interaction sites (boxed) between LH1- α and RC at the periplasmic side. **b**, Interaction sites (boxed) between LH1- α and RC at the cytoplasmic side. The letters in the boxed areas in **a** and **b** correspond to the panels in **Extended Data Fig. 6**. Color codes for panels **a** and **b**: magenta, L-subunit; marine, M-subunit; green, C-subunit; yellow, H-subunit; light grey, LH1 α/β -subunits **c**, Interactions

between adjacent LH1 α - α and α - β subunits. Color codes for panel **c**: magenta and dark cyan, LH1 α -subunits; yellow and cyan, LH1 β -subunits; green, Bchl; light yellow, Spx.

Figure 5 | Calcium-binding sites in the LH1 complex. **a**, Binding pattern of 16 Ca^{2+} ions in LH1. Green, LH1 α -subunits; blue, LH1 β -subunits. **b**, The positions of two Ca^{2+} ions in the LH1 subunits. Ca^{2+} and BChl *a* are represented by red spheres and green sticks respectively. **c**, A close-up view of the Ca^{2+} -binding site. The α -subunit is depicted in green, and the β -subunit in pink. **d**, Top view of the expanded region of the Ca^{2+} -binding site.

Figure 1

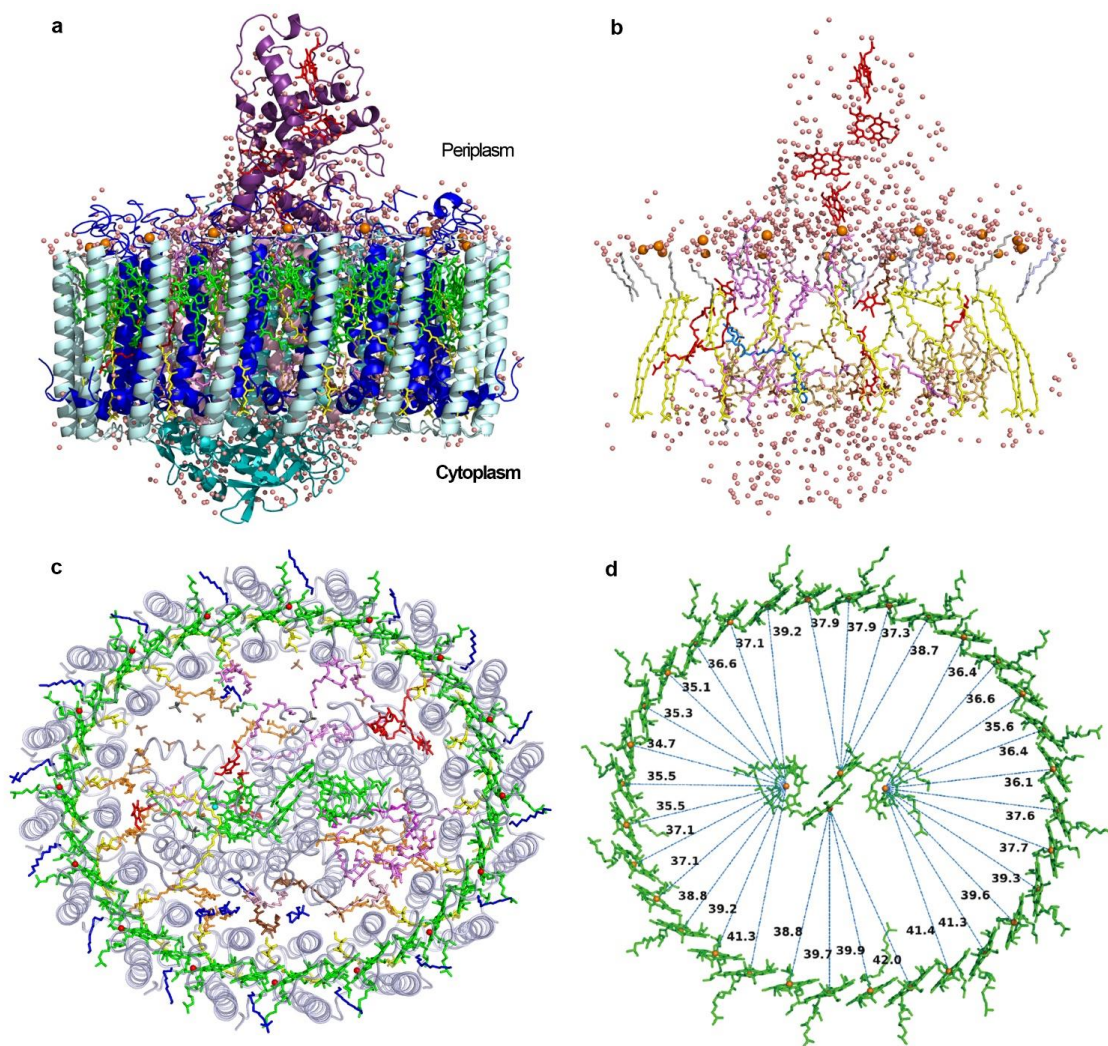


Figure 2

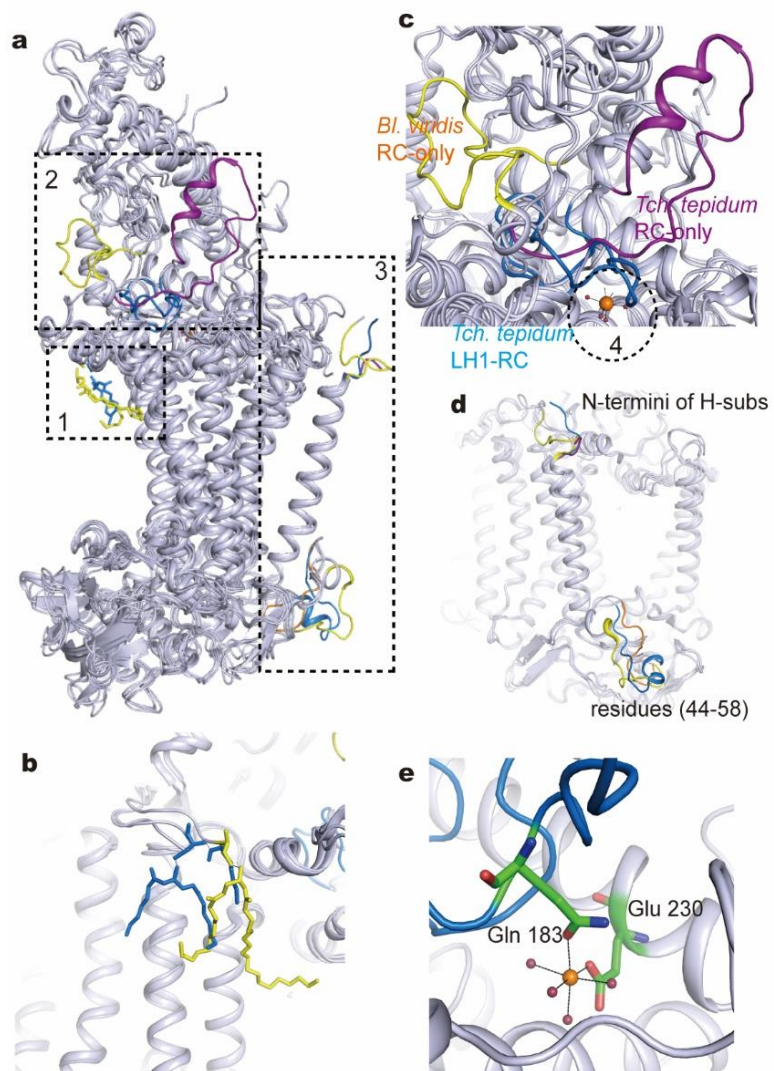


Figure 3

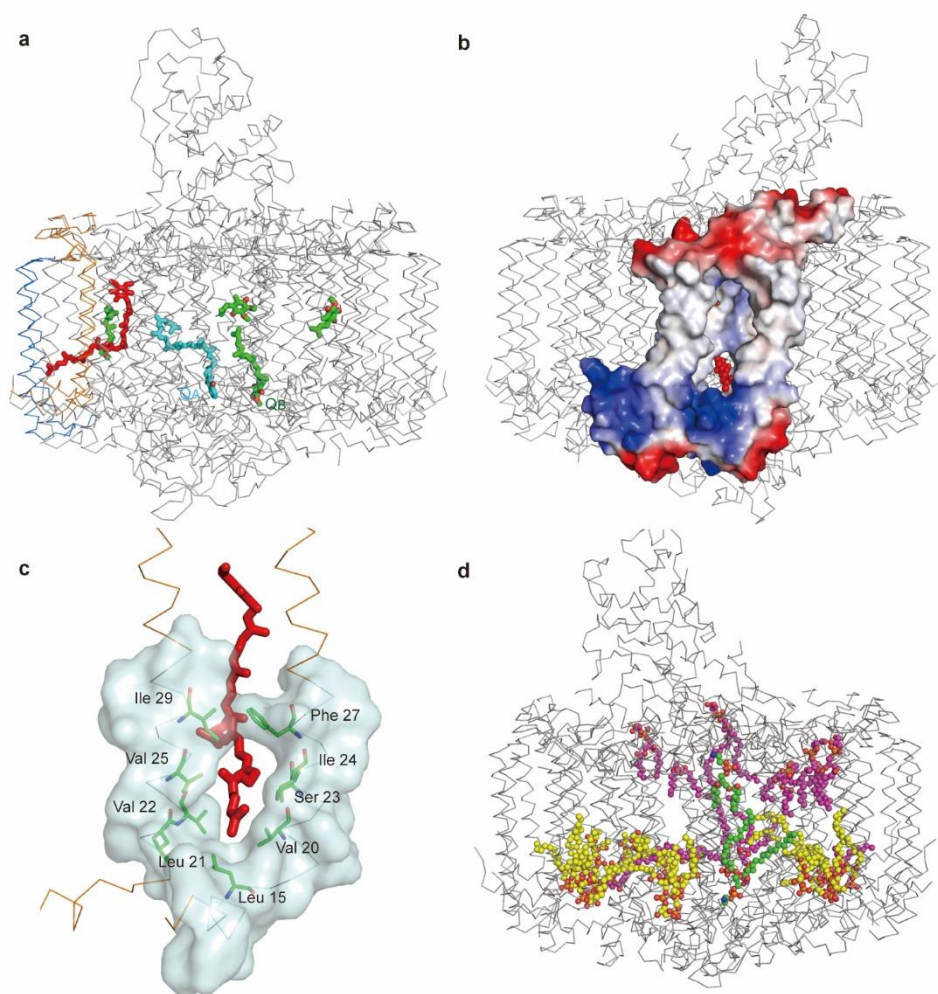


Figure 4

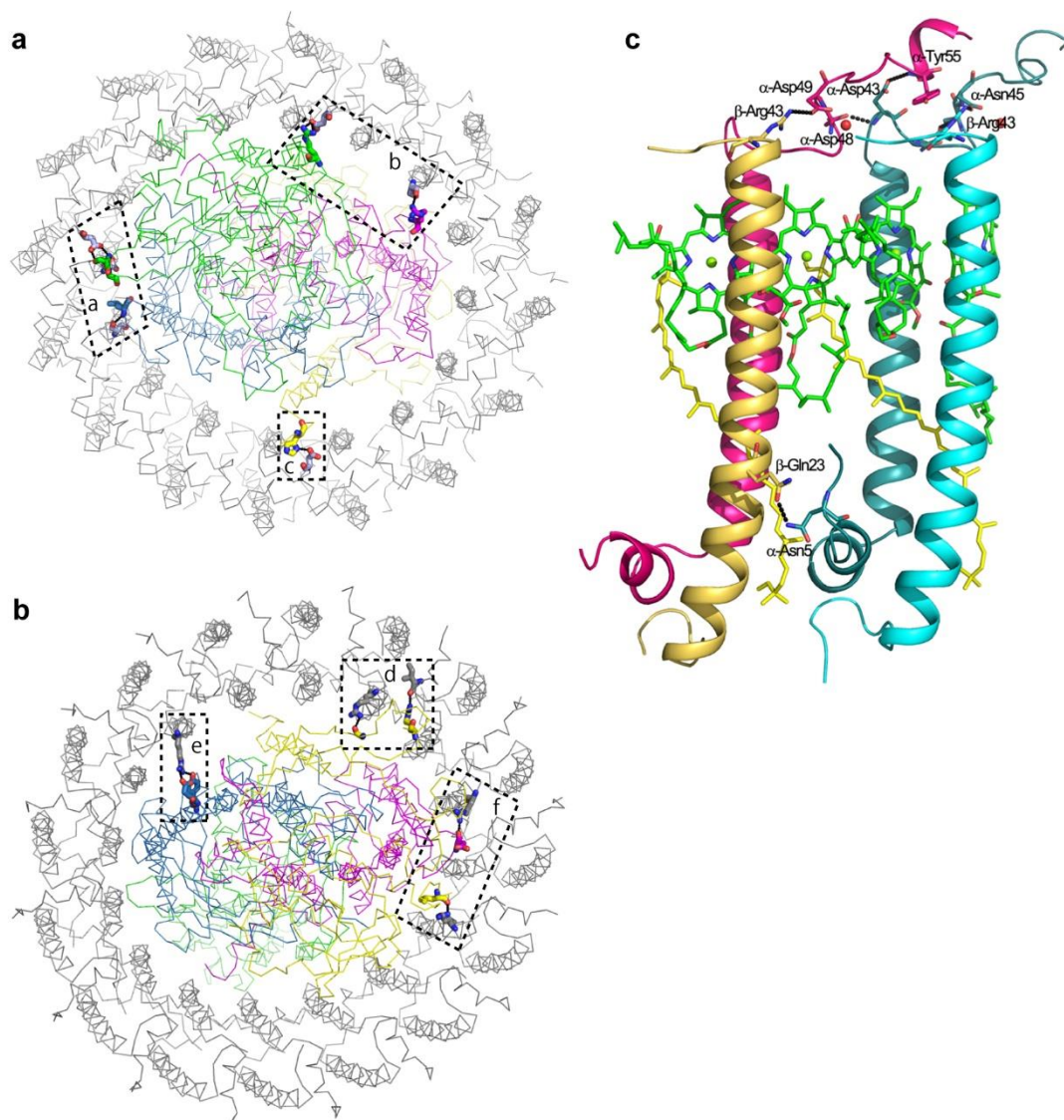
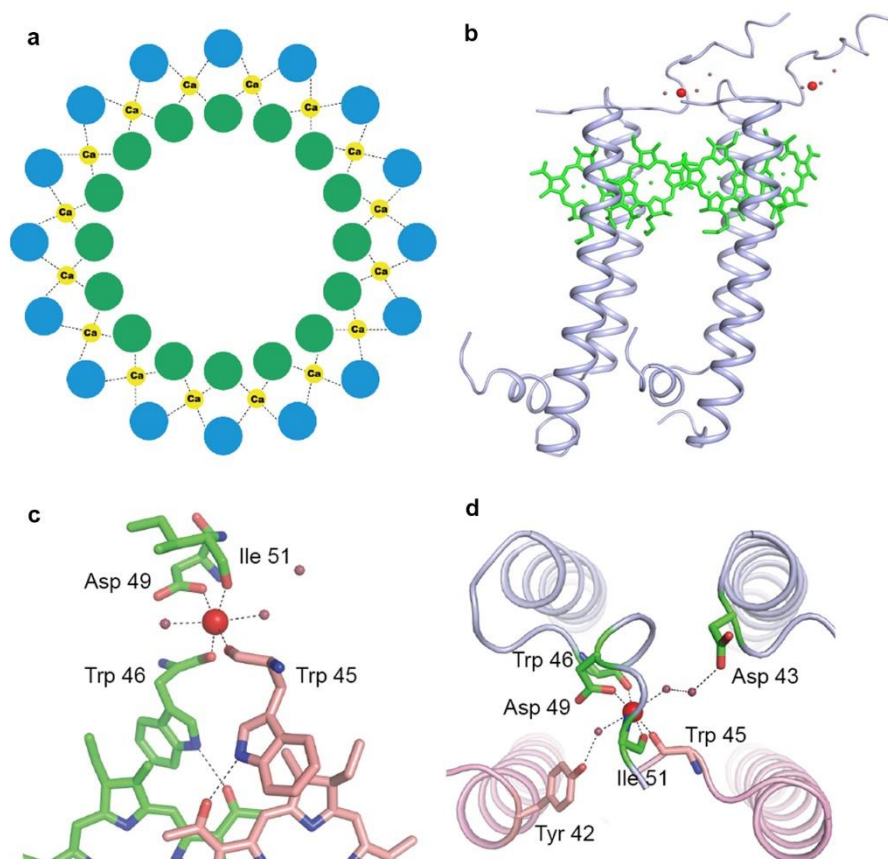


Figure 5



METHODS

No statistical method was used to predetermine the sample size. The experiments were not randomized, and the investigators were not blinded to allocation during experiments and outcome assessment.

Purification and crystallization

Tch. tepidum cells were grown in a growth chamber (BiOTRON, LH-410PFP-SP, NK System, Japan) at 49°C for 7 days. The light illumination was provided by LED lamps specified for plant growth, which have emission peaks at around 450 nm and 645 nm, respectively, at a light intensity of 30 $\mu\text{Einsteins m}^{-2} \text{s}^{-1}$. The bacterial cells grown under this condition appeared to have a larger ratio of LH1-RC/LH2 according to the absorption spectra, which suggests that there are more LH1-RC in the same amount of wet bacterial cells. LH1-RC complex was purified as described previously^{2,28} with slight modifications. The final LH1-RC samples with a ratio of A_{915}/A_{280} over 2.20 were collected and precipitated by addition of polyethylene glycol 1,450 to a final concentration of 13% (w/v), and then suspended in 20 mM MES (pH 6.2) containing 3.4% *n*-octylphosphocholine (OPC) to a concentration of 20 mg protein ml^{-1} . Crystallization was performed by a microbatch-under-oil method in which, 2 μl of the above protein solution was mixed with an equal volume of the precipitant solution containing 50 mM MES (pH 6.2), 50 mM CaCl_2 , 10 mM MgCl_2 , 3.4% OPC and 26% polyethylene glycol 1,450. The crystals grew to sizes of $0.3 \times 0.4 \times 0.05 \text{ mm}^3$ to $0.4 \times 0.8 \times 0.2 \text{ mm}^3$ in 10 days at 20°C (Extended data Fig. 1a), which were then transferred into a 10 μl cryoprotectant solution containing 50 mM MES (pH 6.2), 3.4% OPC, 30% polyethylene glycol 1,450, 50 mM CaCl_2 and 15% glycerol, and flash-frozen immediately in a nitrogen stream.

Data collection

X-ray diffraction experiments were carried out at beamlines BL41XU of SPring-8 and BL1A of the Photon Factory (Japan), and the highest resolution diffraction data used for structural analysis was collected at BL41XU of SPring-8. The wavelength of X-rays used was 1.0 Å and the beam size was $35 \times 22 \mu\text{m}^2$. The diffraction images were recorded with a Pilatus 6M detector, and the crystals were rotated by 0.1° in a helical manner. A total of 5,400 images covering a rotation angle of 540° were collected. The photon flux of the beamline used was 6.8×10^{11} photons s^{-1} (after attenuation by a 0.75-mm thick aluminium), and the exposure time was 0.1 s for each diffraction image. The diffraction data was processed, integrated and scaled using the XDS Program Package (version October 15, 2015)²⁹, and the reflection data statistics are summarized in Extended Data

Table 1.

Structure refinement

The initial structure of the LH1-RC complex was solved by the molecular replacement method using the Phaser program in PHENIX (version 1.12-2829)³⁰. The structure of LH1-RC previously determined at 3.0 Å resolution from *Tch. tepidum* (PDB code: 3WMM) was used as the search model, with the Ca²⁺ ions, lipid and solvent molecules omitted. Five percent of reflections were used for the free *R* factor calculation in the structure refinement. The initial model was subjected to rigid body and restrained refinements successively in a resolution range 50-2.0 Å. Incorporation of cofactors, lipid and detergent molecules and model modification were performed using COOT (version 0.8.2)³¹. For the assignment of lipid molecules, positions of the phosphorous atoms in lipids were confirmed either by the strong electron density interacting with the positively charged amino acid residues or the peaks found in the anomalous map. The lipids were assigned, based on the electron density of the polar head group, as CDLs when they were connected to each other, and as PEFs and PGs when they interact with the negatively charged amino acids and neutral groups, respectively. Positional and isotropic displacement parameters were refined in the resolution range of 50-1.9 Å. After solvent molecules were included in the model, anisotropic displacement parameters were refined, and the final model was refined to $R_{\text{work}} = 18.15\%$ and $R_{\text{free}} = 21.52\%$, with 98.42% residues in the favored Ramachandran region, 1.51% in the allowed region, and 0.08% in the outliers. The relatively high *R* values may be caused by blurred electron densities at the terminal regions of the LH1 polypeptides, especially the N-terminus, resulting in higher *B*-factors in these regions. In addition, some residual densities in the gap region between RC and the LH1 ring were not modelled, which may be flexible fragments of lipids and quinones. The refinement statistics are listed in Extended Data Table 1, and the quality of the structure was analyzed by using PROCHECK³². Figures were made with the PyMOL program³³. The atomic coordinates and structural factors were deposited in Protein Data Bank under accession code 5Y5S.

28. Suzuki, H. *et al.* Purification, characterization and crystallization of the core complex from thermophilic purple sulfur bacterium *Thermochromatium tepidum*. *Biochim Biophys. Acta* **1767**, 1057-1063 (2007).
29. Kabsch, W. Xds. *Acta Cryst. D* **66**, 125-132 (2010).
30. Adams, P. D. *et al.* PHENIX: a comprehensive Python-based system for macromolecular structure solution. *Acta Cryst. D* **66**, 213-221 (2010).

31. Emsley, P., Lohkamp, B., Scott, W. G. & Cowtan, K. Features and development of Coot. *Acta Cryst. D* **66**, 486-501 (2010).
32. Laskowski, R. A., Macarthur, M. W., Moss, D. S. & Thornton, J. M. Procheck - a program to check the stereochemical quality of protein structures. *J. Appl. Cryst.* **26**, 283-291 (1993).
33. Schrodinger, LLC. *The PyMOL molecular graphics system, Version 1.8* (2015).

Legends for Extended Data Figures

Extended Data Figure 1 | Quality of the LH1-RC crystal and its packing pattern. a, An image of the LH1-RC crystals obtained in the present study. These crystals were obtained reproducibly with the present crystallization conditions. **b,** A typical diffraction image of the LH1-RC crystal taken at BL41XU of SPring-8, Japan, with a wavelength of 1.0 Å at 100 K. This diffraction image was obtained reproducibly with many crystals tested. **c, d,** Packing pattern of the previous (**c**) and present crystal (**d**).

Extended Data Figure 2 | Close-up views of the electron density maps for some of the cofactors of LH1-RC. The blue mesh represents 2Fo-Fc map contoured at 1.0 σ , taken at a wavelength of 1.0 Å and analyzed to 1.9 Å resolution. **a-d,** The special pair BChls (**a**) and one pair of the LH1 BChls (**b**), one of the CDL (**c**) and the Q_B molecule (**d**).

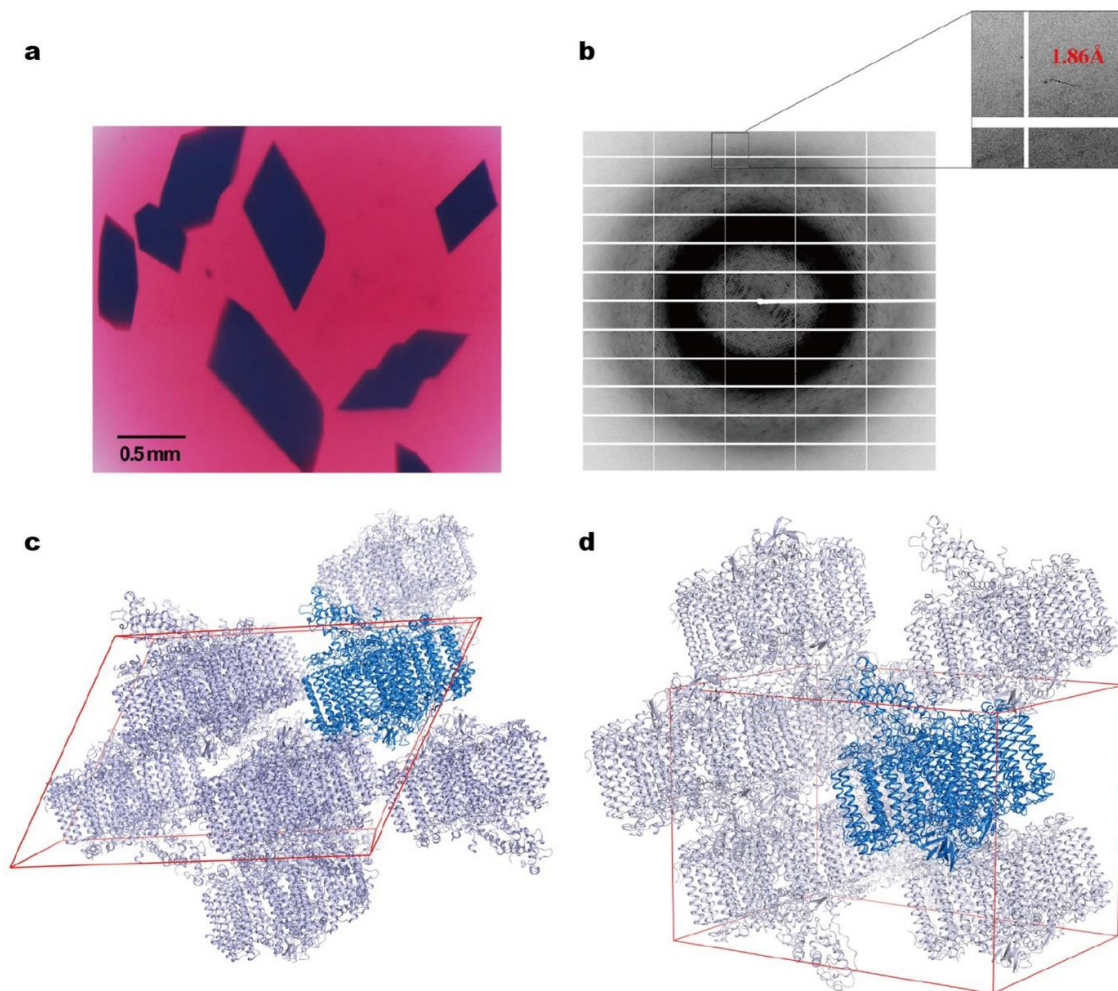
Extended Data Figure 3 | Comparison of the arrangement of the cofactors between the previous and present structures. a, Arrangement of the cofactors in the previous 3.0 Å structure, with a view from the top of the membrane. **b,** Superposition of the cofactors between the previous 3.0 Å and present 1.9 Å structures. **c,** The same as panel **b**, with the view from the side of the membrane. In panels **b** and **c**, the cofactors revealed in the present 1.9 Å structures were colored differently, whereas those in the previous 3.0 Å structures were depicted in grey.

Extended Data Figure 4 | Comparison of the protein structures between the previous and present structures. a, Superposition of the RC subunits between the previous 2.2 Å and present 1.9 Å structures, with a side view from the membrane plane. **b,** Superposition of the RC subunits between the previous 3.0 Å and present 1.9 Å structures, with a side view from the membrane plane. **c and d,** Superposition of the LH1 subunits between the previous 3.0 Å and present 1.9 Å structures, with a side view (**c**) and top view (**d**) relative to the membrane plane, respectively. In all panels, the present 1.9 Å structure is colored, whereas the previous structures are depicted in grey.

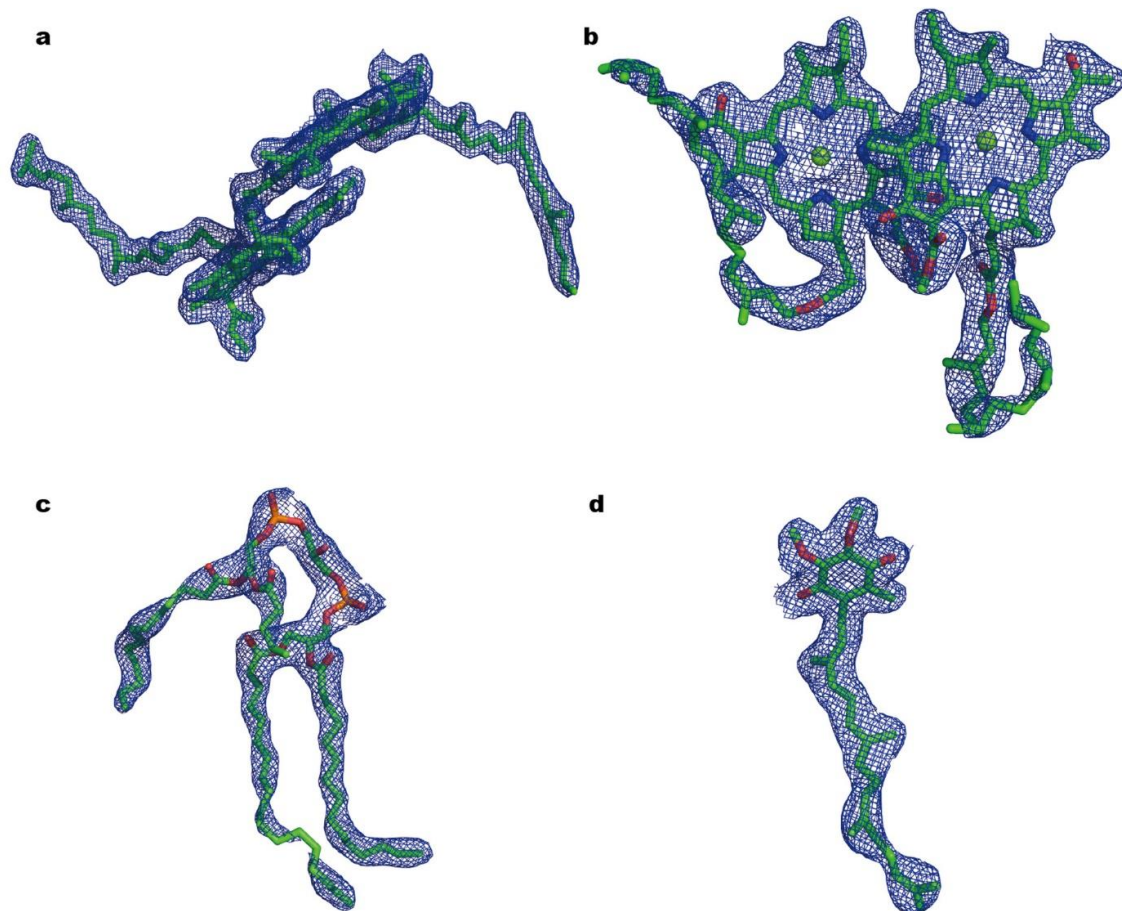
Extended Data Figure 5 | Hydrogen-bond networks for the protonation of Q_B. **a**, Two possible proton channels connecting Q_B to the cytoplasmic surface. Thick arrow (colored in marine) indicates the main channel formed within the H-subunit, which is enlarged in panel **b**, and the thin arrow indicates the second channel. **b**. The main hydrogen-bond network indicated by the thick arrow in panel **a**, formed by a number of water molecules and the residues (green) from the H-subunit (pale cyan). Q_A and Q_B are depicted in violet and red, respectively, and the non-heme iron is depicted in deep purple. The hydrogen bonds are depicted as dashed lines, and water molecules participating in the hydrogen-bond networks are depicted in orange, whereas those not participating are depicted in grey.

Extended Data Figure 6 | Protein-protein interactions between LH1 and RC. **a, b, c**, Interactions between the LH1 α -subunits and RC subunits at the periplasmic side. These three panels correspond to those indicated in the boxed areas in Fig. 4 of the main text. **d, e, f**, Interactions between the LH1 α -subunits and RC subunits at the cytoplasmic side, with each of the panels corresponding to those indicated in the boxed areas in Fig. 4 of the main text.

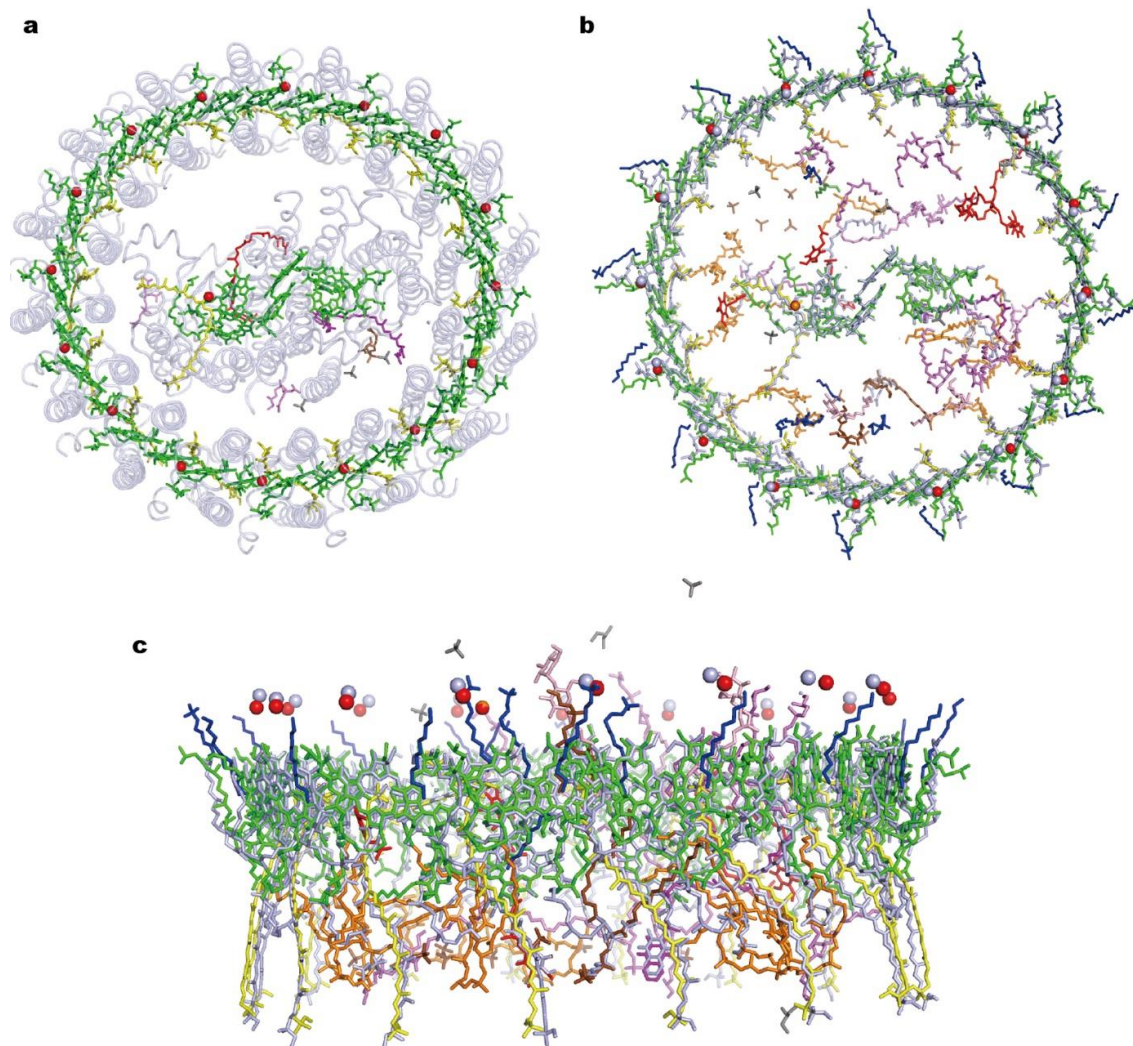
Extended Data Figure 1



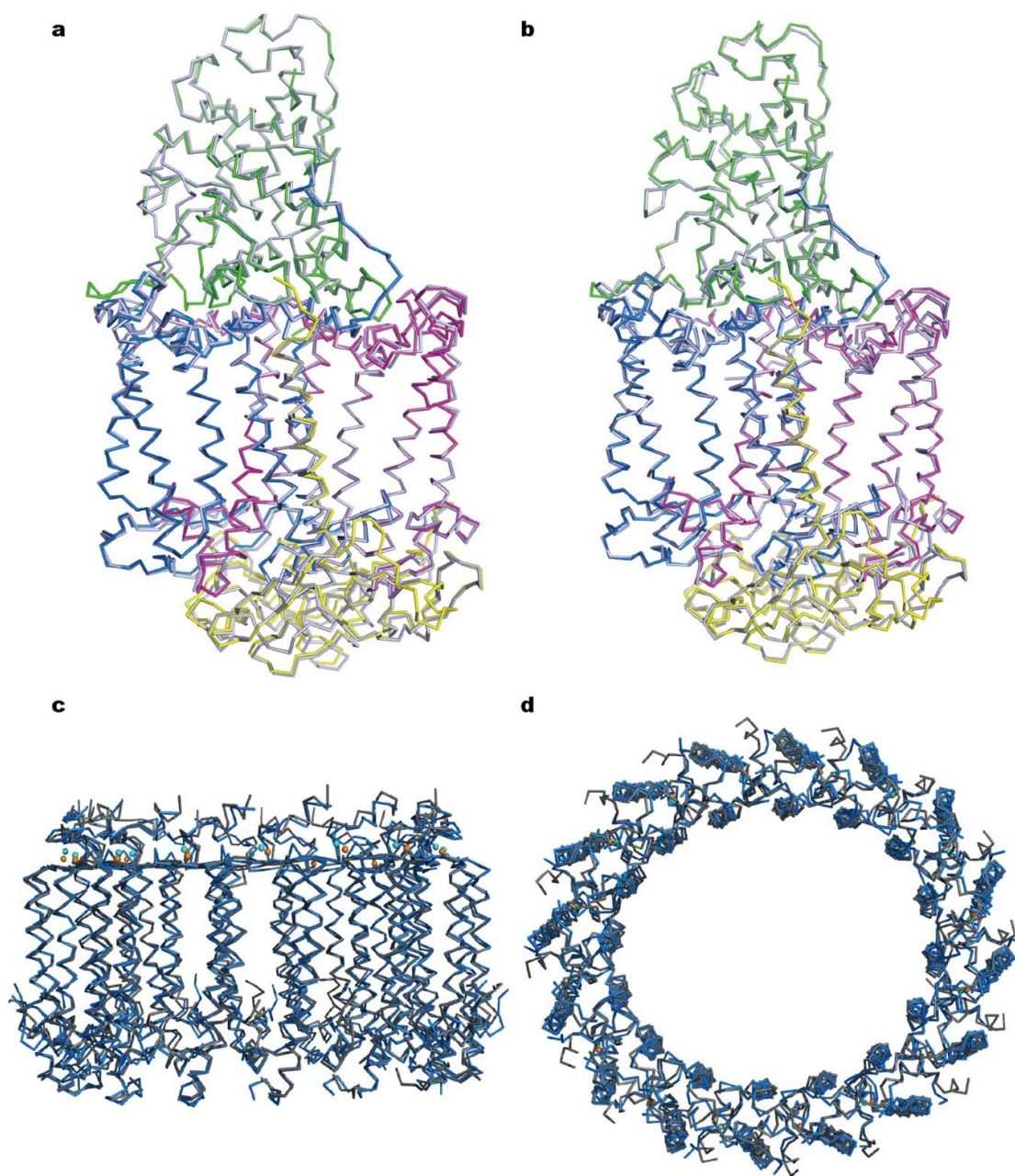
Extended Data Figure 2



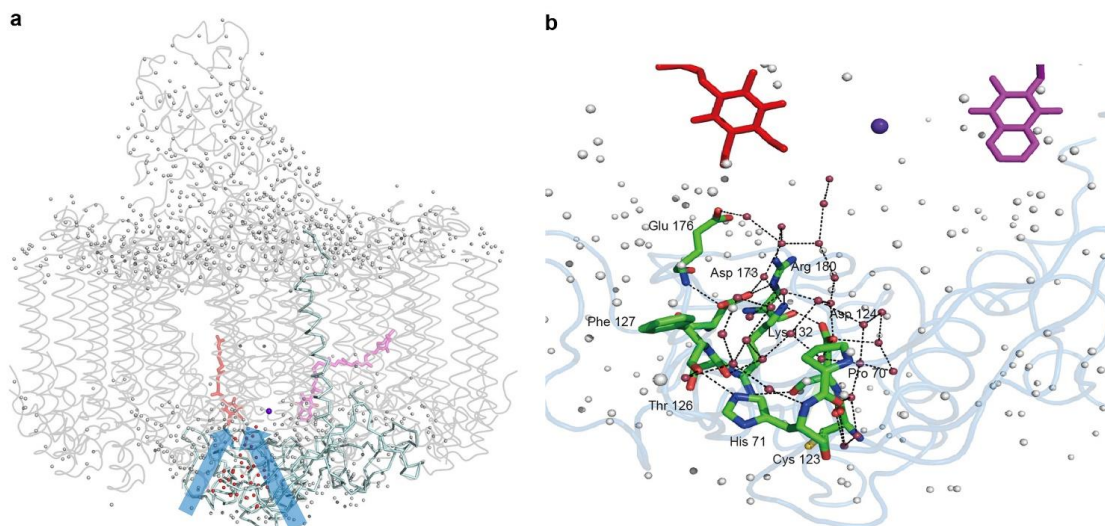
Extended Data Figure 3



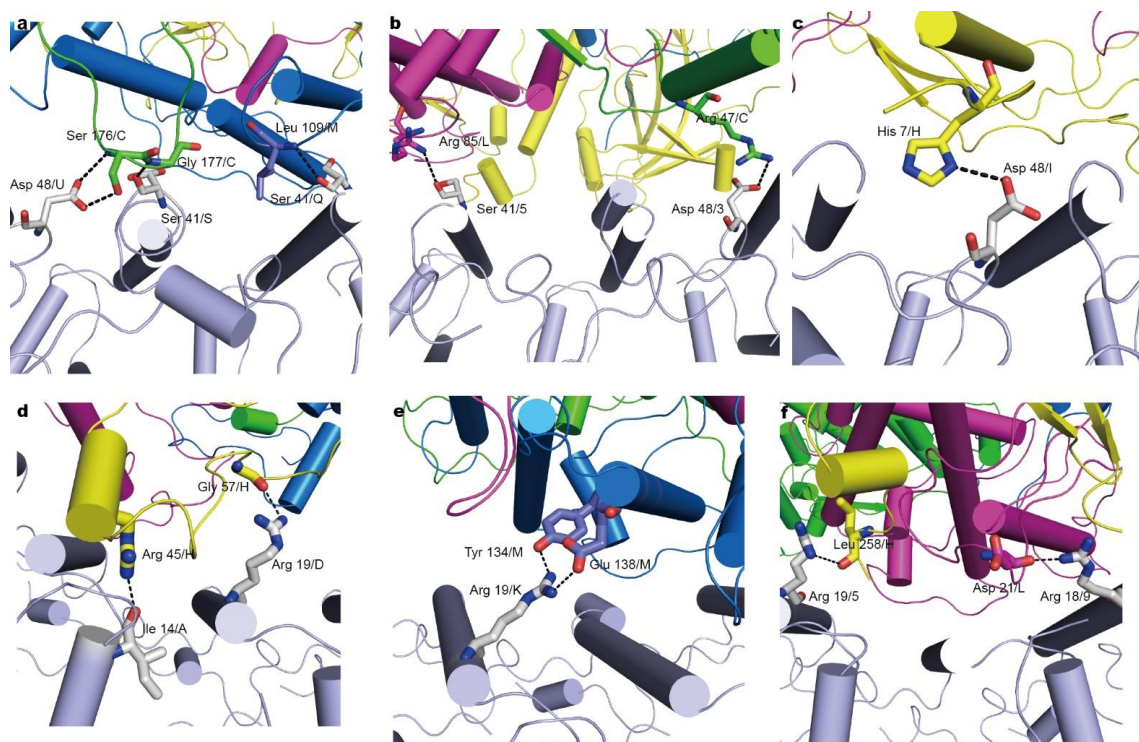
Extended Data Figure 4



Extended Data Figure 5



Extended Data Figure 6



Extended Data Table 1 | Data collection and refinement statistics.

	LH1-RC
Data collection	
Space group	C121
Cell dimensions	
<i>a</i> , <i>b</i> , <i>c</i> (Å)	145.23, 143.81, 210.28
α , β , γ (°)	90.00, 90.74, 90.00
Resolution (Å)	46.92-1.90 (1.968-1.900)*
<i>R</i> _{merge}	0.1035 (1.863)
<i>I</i> / σ <i>I</i>	9.47 (1.14)
Completeness (%)	99.95 (99.94)
Redundancy	9.2 (8.0)
Refinement	
Resolution (Å)	46.92-1.90 (1.968-1.900)*
No. reflections	338536 (33812)
<i>R</i> _{work} / <i>R</i> _{free}	0.1815 (0.3558)/0.2152 (0.3737)
No. atoms	
Protein	22003
Ligand/ion	5022
Water	956
<i>B</i> -factors	
Protein	63.68
Ligand/ion	73.62
Water	63.26
R.m.s. deviations	
Bond lengths (Å)	0.018
Bond angles (°)	1.77

*Values in parentheses are for highest-resolution shell.

The table was prepared by using PHENIX with all automatic default settings.

**Extended Data Table 2 | Components of LH1-RC
determined at the 1.9 Å resolution.**

	Proteins	Cofactor	Numbers
RC	C, H, M, L	BChl <i>a</i>	4
		BPhe <i>a</i>	2
		Heme-Fe	4
		Spirilloxanthin	1
		Non-heme-Fe	1
		Mg	1
		MQ8	1
		UQ8	5
		CDL	9
		PG	10
		PEF	2
LH1	α (16) β (16)	BChl <i>a</i>	32
		Spirilloxanthin	16
		Ca	16
Total	36		104

Extended Data Table 3 | Average B-factors of the RC subunits and α -/ β -apoproteins of LH1.

LH1 α -apoproteins	No. of atoms	Average B-factors
A	548	72.17
D	559	75.37
F	559	79.27
I	574	75.90
K	571	69.46
O	569	62.35
Q	571	56.56
S	582	60.01
U	580	65.40
W	565	67.74
Y	571	74.25
1	564	79.34
3	569	78.86
5	548	72.61
7	566	72.46
9	571	72.36
Average		70.83

LH1 β -apoproteins	No. of atoms	Average B-factors
B	417	80.85
E	392	84.21
G	417	89.55
J	417	82.48
N	417	74.38
P	417	64.49
R	411	60.12
T	426	64.16
V	417	73.47
X	411	77.82
Z	403	79.47
2	411	84.72
4	417	80.31
6	417	74.92
8	411	76.65
0	426	76.71
Average		76.47

RC subunits	No. of atoms	Average B-factors
C	2590	51.82
L	2466	44.45
M	2850	43.60
H	1976	60.59
Average		49.36

Extended Data Table 4 | Interactions between LH1 and RC.

Periplasmic side	
LH1- α	RC
Protein-Protein	
Asp48/3	Arg47/C
Ser41/5	Arg85/L
Asp48/I	His7/H
Ser41/S	Gly177/C
Asp48/U	Ser176/C
Ser41/Q	Leu109/M
Protein-Lipid	
Asp48/1	PGV34/a
Asn45/1	
Asp48/5	PGV39/a
Ser41/A	PGV31/a
Asn45/D	
Leu40/D	
Asn45/K	PEF304/a
Leu40/K	

LH1- α	LH1- α
Asp43	Asp48
	Ser54
	Tyr55
	Gln56
Asn45	Gln56

LH1- α	LH1- β
Leu44	Arg43
Asn45	
Asp49	
Tyr55	Pro44

LH1- β	LH1- β
Tyr42	Leu46

Cytoplasmic side	
LH1- α	RC
Protein-Protein	
Arg19/5	Leu258/H
Arg18/9	Asp21/L
Ile14/A	Arg45/H
Arg19/D	Gly57/H
Arg19/K	Tyr134/M
	Glu138/M
Protein-Lipid	
Arg19/9	PGV40/a
Arg18/A	
Arg19/A	CDL303/a
Ile14/A	CDL/30/a
Arg18/D	
Arg19/D	
Ser23/F	CDL25/a
Arg19/K	CDL27/a
Arg18/O	
Ser23/O	PEF12/a
Arg19/O	CDL28/a
Asp16/Q	CDL29/a
Arg19/S	
Arg19/U	CDL24/a
Arg18/Y	CDL26/a
Arg19/Y	

LH1- α	LH1- β
Tyr9	Asp11
Lys10	
Trp12	Thr7
Leu13	